New Morphometric Data of Lunar Sinuous Rilles

Sabrina Podda, Maria Teresa Melis, Claudia Collu, Valentino Demurtas, Francesco Onorato Perseu, Maria Teresa Brunetti, and Marco Scaioni

***Abstract*—On the surface of the Moon a large number of linear features are recognizable. Long and narrow depressions are defined as lunar rilles. Their morphology has different characteristics, related to their origin. Among these, the sinuous rilles represent lineaments considered remnants of shallow lava channels. In this article, a quadrant of the Moon has been analyzed to recognize and map this type of morphology. An accurate morphometric analysis has been accomplished, using the lunar reconnaissance orbiter camera which has a resolution of 100 m/pixel, and the digital elevation model from lunar orbiter laser altimeter with a resolution of 6 m/pixel. A total of 51 sinuous rilles have been recognized in the study area, 18 of which are new, improving a previous catalogue. The resulting quantitative and qualitative measurements were analyze and compared each other' to identify potential morphological trends. Different relationships between morphological parameters have been proposed, and the results enhance the importance of substrate composition in the evolution of these features, emerged mainly from the variations in width and depth values. The linear relationship between these two parameters is consistent with the idea that erosion efficiency acts proportionally in both vertical and horizontal directions. Partial filling phenomena by subsequent lava flows probably occurred in some sinuous rilles located in maria. The hypothesis of a constructive genesis requires further investigation to identify the levees created by sinuous rilles' formation process.**

***Index Terms*—Moon, lunar sinuous rilles, volcanic activity.**

I. Introduction

LUNAR sinuous rilles are enigmatic lineaments that would represent the remnants of shallow lava channels [1], [2], or collapsed subsurface lava tubes [3]–[6]. On lunar surface, sinuous rilles are generally located in *maria* regions, and they are often associated with depressions of different morphologies, interpreted as potential source vents [6]. These particular lava channels are characterized by highly varying depths and widths with parallel, laterally continuous walls, that exhibit variable degrees of sinuosity (see Fig. 1). The origin of sinuous rilles is still debated, particularly in regards to whether these channels originated by constructive or erosive processes [7]. This discussion is open also to other planets, where similar features have been recognized, i.e., Mars, Venus, and the Jupiter's Moon, Io [8]–[10], [11].

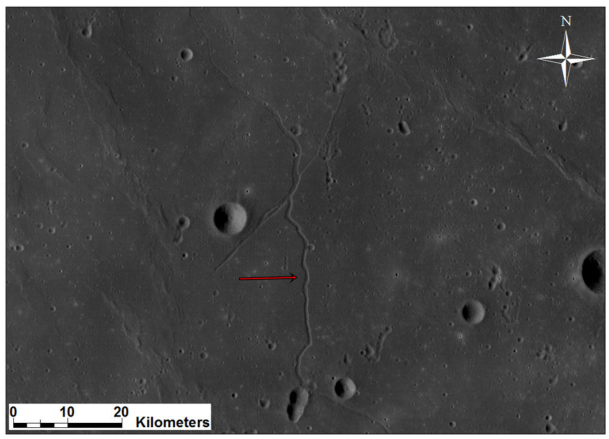

Fig. 1. Example of a sinuous rille observed on the Moon. Sinuous rilles are probably the remnants of shallow lava channels (e.g., the feature in this WAC—image is centered at 2.0° N, 27.1° E).

In the last years, these morphologies, and in general, the surficial features of the Moon, received a new attention, as they can be connected with the presence of lava tubes on the lunar surface and with possible sites for human landing and activities [12]–[16].

A constructive origin would generate sinuous rilles as the result of differential cooling of lava flow, which would create leeves channelizing the flow into a built channel [17]. In this way, rather shallow open channels or deeper underground channels (lava tubes) would have formed. Lava tubes are detectable on the lunar surface only if they have undergone a collapse of the roof. The alignment of several collapses likely generates the so-called skylights, which however cannot be considered sinuous rilles, because they lack the typical characteristics of these morphologies, such as sinuosity and parallel laterally continuous walls.

Erosional origin is further divided into thermal and mechanical erosive processes [1], [6], [18], [19]. Mechanical erosion would occur as a result of the collision between lava flow particles and substrate particles. Thermal erosion, on the other hand, occurs when the temperature of the lava flow is his higher than

Manuscript received March 8, 2020; revised June 2, 2020; accepted June 14, 2020. Date of publication June 17, 2020; date of current version June 25, 2020. This work was support in part by the Italian Space Agency (ASI) Science Data Center (ASDC) and the Chinese Center for Space Exploration (COSE) and in part by the framework of the Joint Lunar Map Drawing Project "Moon Mapping". *(Corresponding author: Maria Teresa Melis.)*

Sabrina Podda, Maria Teresa Melis, Claudia Collu, and Valentino Demurtas are with the Department of Chemical and Geological Sciences, University of Cagliari 09042, Monserrato, Italy (e-mail: sabrinap91@hotmail.it; titimelis@unica.it; claudiacollu26@yahoo.it; v.demurtas4@tiscali.it).

Francesco Onorato Perseu is with the CIREM, University of Cagliari 09123, Cagliari, Italy (e-mail: fra.perseu@gmail.com).

Maria Teresa Brunetti is with the Research Institute for Geo-Hydrological Protection–Italian National Research Council, 06128 Perugia, Italy (e-mail: mariateresa.brunetti@irpi.cnr.it).

Marco Scaioni is with the Department of Architecture, Built Environment and Construction Engineering, Politecnico di Milano 20133, Milano, Italy (e-mail: marco.scaioni@polimi.it).

This article has supplementary downloadable material available at http://ieeexplore.ieee.org, provided by the authors.

Digital Object Identifier 10.1109/JSTARS.2020.3003080

the melting point of the substrate. Thermal erosion preferably occurs if the slope of the lunar surface is less than 3.5°, since the low gravity value is not sufficient to produce the kinetic energy capable of driving mechanical erosion [2]. These two processes of erosion could be associated with the changes in depth along the channel. The depth of a thermally-eroded channel shows a decreasing with increasing distance from the source, while the depth of a mechanically eroded channel is highly variable along the channel [8], [20].

Constructive and erosive processes are also associated with different eruptive styles. Sinuous rilles resulting by erosive processes are generated from turbulent lava flows, high effusion rates, and prolonged eruptions lasting several months or years. Instead, a constructive origin is associated with less turbulent flows and stationary effusion rates within weeks or months [2], [21]–[23]. The lava composition and its rheological characteristics are also important elements that influence sinuous rilles formation. Indeed, the formation of lava channels by thermal erosion is consistent with high flow volumes of low-viscosity lavas during superheated volcanisms [20]. The model discussed by these authors proposes lavas with the composition of the komatiite, an ultramafic effusive rock, consistent with a very high temperature eruption ($\sim$ 1600 °C).

The early analyses of the distribution and morphology of lunar sinuous rilles, categorized them into two main classes [3], [24].

1) Simple channels, usually with no tributaries.
2) Complex rille systems, with many intersecting or branching sections.

Most of the "complex rille systems" are located in impact craters, which exhibit a typical fractured floor. Their origin is likely the result of tectonic uplift and/or volcanic modification of the lava flooding into the crater floor [25].

A detailed analysis on the origin of the sinuous rilles, with a morphological classification of Rima Marius, is described in [26]. In this article, the term of "*rillette*" is proposed to identify short and narrow rilles connected to the main channel, as generated from the main volcanic source. The authors proposed an evolution of this system of rilles, assigning relative ages to each ones and to relative volcanic layers. The results of this article demonstrate an origin of the rilles based on the evolution of concentrated flows of molten lavas beneath a thin layer of solidified lava crust.

A global map of sinuous rilles identified on the lunar surface, has been produced and discussed in [6]. This map was obtained by considering only those features formed by lava erosion.

The current study aims at updating this catalog of lunar sinuous rilles, in a specific area, to map all typologies of sinuous rilles described earlier. The purpose is to apply a morphometric analysis of these features, as well as to identify any trends useful for a better understanding of sinuous rille formation. Indeed, the morphological features can support the geological models to understand the origin (thermal/ mechanical erosion or constructional), and the dynamics of evolution based on rheological characteristics of the lavas and the geological substratum.

The major objectives of this article are as follows.

1) To add new data to the existing map of sinuous rilles, in a region of the lunar near side, and systematically document them.
2) To analyze the morphometric parameters of each rille, and compare them each other.
3) To use the mapped rilles and their morphological characteristics to discuss the proposed models of their origin, and the parameters controlling the dynamics and the interaction with the geological substratum.

II. Study Area

The study area is a quadrant of the northern hemisphere of the lunar nearside, between 0°E to 90°E longitude and 0°N to 60°N latitude (see Fig. 2). It is characterized by geological units of different time periods, as indicated in the geological map of the study area (see Fig. 3). This map is extracted from the unified global geologic map of the Moon at 1:5,000,000-scale [27]. In this map, the 43 geological units recognized on the entire Moon surface are grouped into the following classes: materials of craters, basins, terra, plains, Imbrium Formation, Orientale Formation, and volcanic units. In the map, sinuous rilles described in this article, are overlaid.

The western region of the study area is dominated by the "dark materials" (i.e., *maria* deposits) with four maria: Mare Serenitatis, Mare Tranquillitatis, Mare Vaporum, and Mare Crisium. The eastern side is mainly made up of highlands deposits, called "terra and plains." This subdivision is also reflected in a different age of the outcrops: the western sector is broadly younger than the eastern one. Furthermore, the whole area is also characterized by "crater materials," which represent distinct geological units deriving from impact craters. The three typologies of deposits date from different periods, and refer to the time-stratigraphic nomenclature proposed in [27] and [28].

1) Dark materials (maria and basins) from the Imbrian and Eratosthenian epochs.
2) Terra and plains from pre-Imbrian and Imbrian epochs.
3) Crater materials from pre-Imbrian, Imbrian, Eratosthenian and Copernican epochs.

Moreover, the lunar surface is covered by the regolith, a thin layer ($<$ 15 m) of fine material, exposed to a continuous particle bombardment [29], [30].

The highlands region appears rugged with numerous impact craters and circular basins of varying size. The maria region seems smoother when compared to the highlands regions. But this condition is valid only at the global scale. On the regional scale these maria regions appear also as rugged terrain. Moreover, tectonic features such as graben and wrinkle ridges, and volcanic morphologies (domes, sinuous rilles and probable skylights) originated mainly in the maria (see Fig. 4).

III. Data and Methodology

The detection, classification and mapping of sinuous rilles have been achieved with the geographic mapping software program ESRI ArcMap, using the global morphologic map and the SLDEM2015 (global lunar digital elevation model) (see Fig. 5). The global morphologic map is the mosaic of the images taken by the wide angle camera (WAC) of the lunar reconnaissance orbiter camera (operated by NASA) with a resolution of 100 m/pixel [31]. The SLDEM2015 is obtained from the

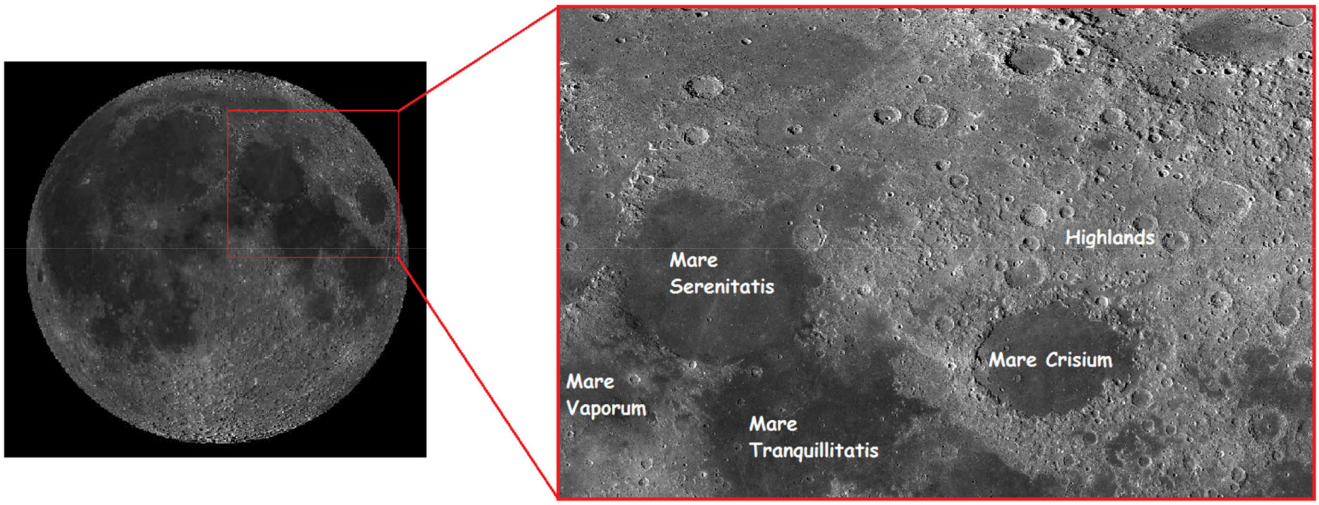

Fig. 2. Study area is located in the northern hemisphere on the lunar nearside, between 0°E to 90°E longitude and 0°N to 60°N latitude: the image of the Moon on the left is a view from LROC Quick Map-ASU (https://quickmap.lroc.asu.edu/), and the box on the right is a WAC image. The area is characterized by numerous *maria*, such as Mare Vaporum, Mare Serenitatis, Mare Tranquillitatis, and Mare Crisium, and by the highlands on the eastern side.

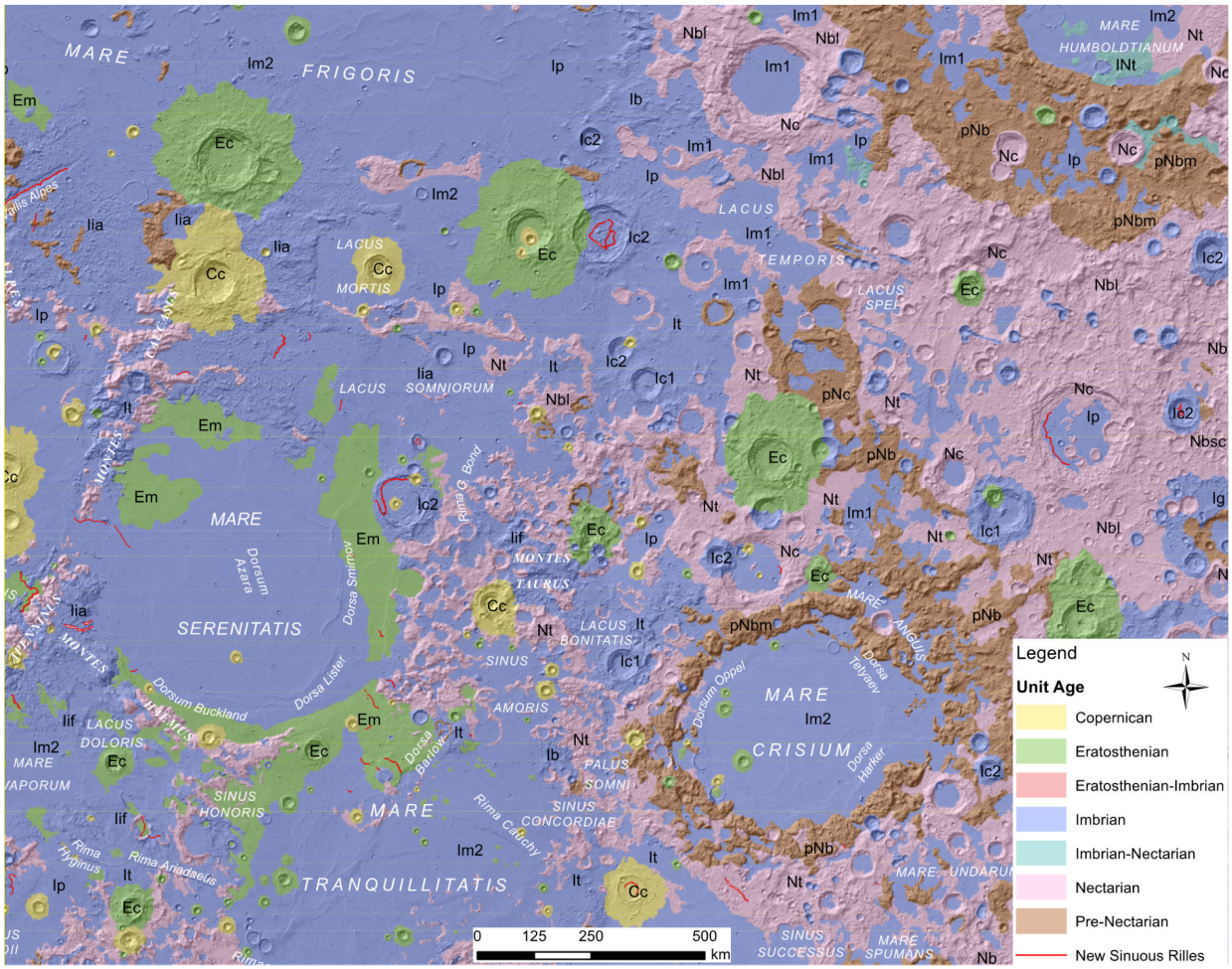

Fig. 3. Geological map of the study area. In the legend, the ages of the units are provided. The new sinuous rilles, mapped in this study, are displayed in red. The black labels are referred to the geological units: **pNc**: pre-Nectarian Crater; **pNb**: pre-Nectarian Basin; **Nt**: Nectarian Terra; **Nbsc**: Nectarian Basin, secondary crater; **Nbl**: Nectarian Basin, lineated; **Nc:** Nectarian Crater; **It**: Imbrian Terra; **Ip**: Imbrian lains; **Im2**: Imbrian Mare, upper; **Iif**: Imbrian Imbrium Fra Mauro Formation; **Iia**: Imbrian Imbrium Alpes Formation; **Ib**: Imbrian Basin, Undivided; **Ic2**: Imbrian Crater, upper; **Ic1**: Imbrian Crater, Lower; **Ic**: Imbrian Crater, Undivided; **Em**: Eratosthenian Mare; **Ec**: Eratosthenian Crater; **Cc**: Copernican Crater [27].

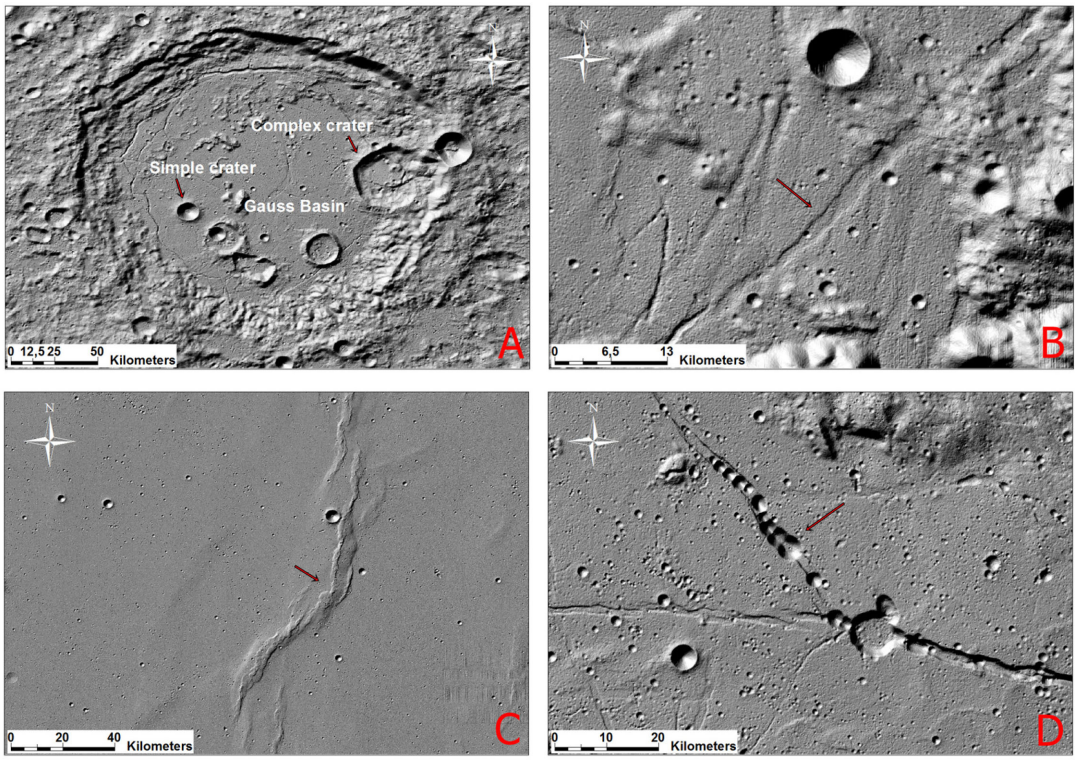

Fig. 4. Images taken from the digital elevation model of the Moon (SLDEM2015) represent different morphologies which characterize the study area. (a) Impact morphologies within the Gauss Basin (feature centered at 36°N, 79°E) such as simple and complex craters [39]. (b) Tectonic graben (centered at 21.3°N, 29.9°E) located at the edge of Mare Serenitatis. (c) Wrinkle ridge (centered at 25°N, 25.4°E) located in Mare Serenitatis. (d) Probable lava tube (centered at 7.7°N, 6.3°E) characterized by roof collapse in different parts of the channel (skylights).

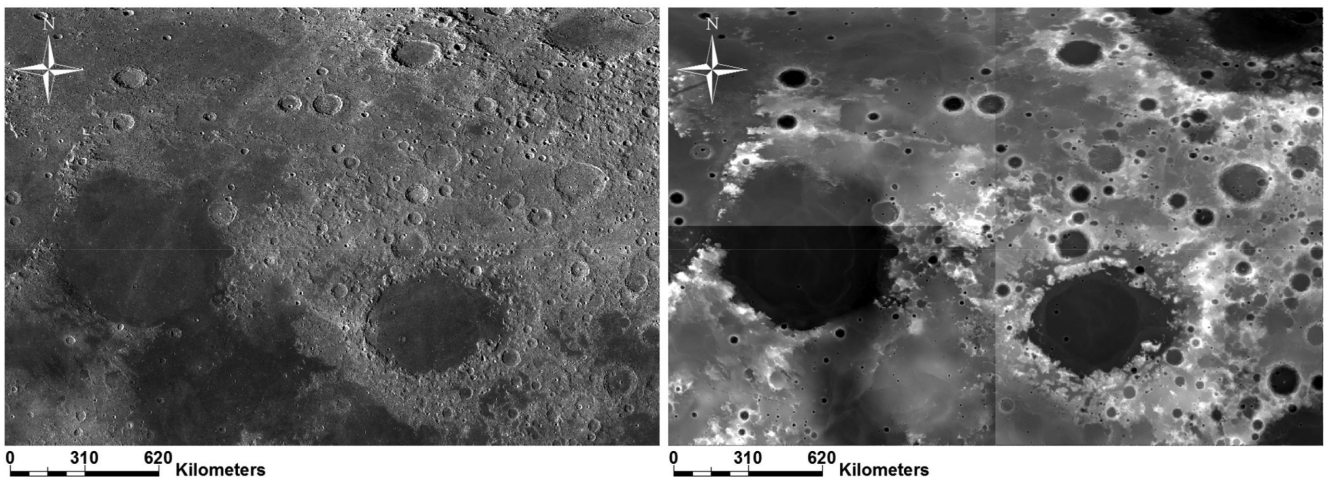

Fig. 5. Images show the data used in the current study: WAC global morphologic map (left) and the SLDEM2015 (right).

combination of lunar orbiter laser altimeter data, and selenological and engineering explorer (SELENE or Kaguya Terrain Camera, operated by the Japan Aerospace eXploration Agency) data. The SLDEM2015 has a resolution of approximately 60 m/pixel and a vertical accuracy of approximately 3–4 m, respectively [32].

Our study is based on a semiautomatic procedure that provides a quantitative analysis of morphologies extracted by visual interpretation. Automatic extraction of landforms is a well-known methodology to obtain quantitative data from DEM and spectral imagery in geological and planetary studies [33]–[36]. Morphometric variables are widely used in geomorphic research supporting models of evolution of landforms [37], [38].

Studying the sinuous rilles, two main characteristics of these features have to be considered: the variability of the shape of these morphologies; and the spatial resolution of the available data.

As described in [6], the sinuous course of these morphologies is the main element that allows us to distinguish them from other structures, which can have similarly continuous and parallel

side walls, but with a rectilinear or gently curved trend, such as grabens [see Fig. 4(b)]. Moreover, the width and the depth of sinuous rilles are very variable along the channel because they may be subject to collapse phenomena and impacts which therefore make them asymmetrical. In this case, the improvement of the interpretation can be provided by the observation of optical data. In some cases, the visual interpretation alone is not sufficient to identify the sinuous rilles, since curved structures have similar characteristics and may often be confused. Therefore, it is useful for this purpose to measure the values of the sinuosity index, which represent a further verification. In this article, all the rilles that showed a sinuosity index lower than 1.03 were excluded, since such a low value is indicative of an arched or rectilinear structure.

Based on the general assumption that the smallest object to be generated by a DEM is at least twice the size of the grid [40], the 100 m resolution cannot be considered satisfactory for the identification of the morphologies, one of the objectives of this research.

The detection of sinuous rilles using WAC and SLDEM has been done, knowing that these morphologies typically are characterized by parallel laterally continuous walls and varying degrees of sinuosity. Moreover, they generally tend to avoid topographic obstructions. Subsequently, all the potential lava channels with these characteristics have been mapped.

On the basis of the recognition and digitalization of the channels, the extraction of the morphometric parameters was done using the DEM. The resulting quantitative and qualitative measurements were analyze and compared each other', to identify potential morphological trends connected to different geological dynamics.

A. Morphometric Features

Measurements of morphological parameters, such as width, depth, length, sinuosity index, regional slope, and azimuth have been collected for each sinuous rille, and they are described in the following.

1) *Width:* Sinuous rille width represents the distance between the top of the two parallel walls of the channel. The method relies on the automatic managing of the elevation profiles obtained on transects orthogonal to the lava channel axis. According to the methodology of [6], width measurements have been acquired at 15 points along the length of each sinuous rille (see Fig. 6). The resulting values have been averaged to get a characteristic width of each rille.
2) *Depth:* Sinuous rille depth is defined as the difference of the mean altitude between the terrain surrounding the channel (i.e., walls elevation) and the bottom of the channel. Altitude values of the walls have been averaged in order to remove local topographic influences. According to the adopted methodology, the depth value has been measured at ten points along the length of each sinuous rille, and then the measurements have been averaged to get a characteristic depth of each rille.

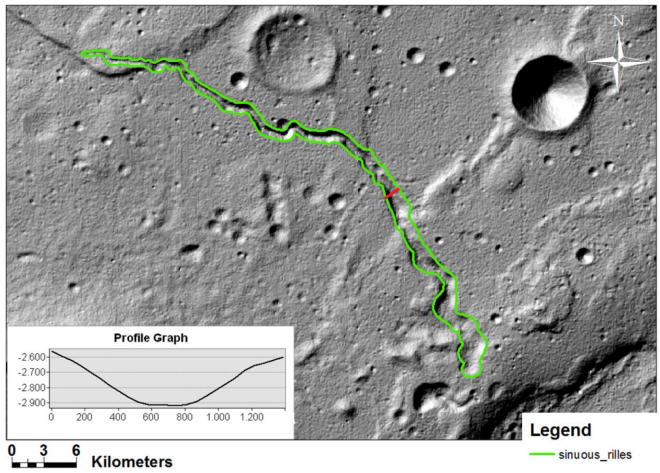

Fig. 6. Image shows the measurement of the width (red bar), perpendicular to the propagation direction of the lava flow. In this sinuous rille the variation of width along the feature is clear.

The points of measures, either for the width and for the depth, were equally spaced. The points overlapping collapse or impact features have been excluded to avoid distortion of the final data.

1) *Length:* Sinuous rille length's was obtained by averaging the lengths of the two walls of the channel, mapped individually.
2) *Sinuosity Index*: This dimensionless quantity is the ratio of the channel length and the distance (straight line) between the start and the end points of the channel. Sinuosity values for terrestrial water channels typically range from 1 (straight course) to 5 (high sinuosity). In this study, the straight distance between the two points of the channel has been calculated creating the minimum bounding geometry enclosing each feature. The value of the longest side of the rectangle has been used as a straight line of the rille (see Fig. 7).
3) *Regional Slope:* it is the slope of the terrain where the sinuous rilles formed, as defined in [6]. This value has been calculated as the ratio of the difference in elevation between the source point and the terminus point of each sinuous rille, and the distance (straight line) between the two points. If the elevation values of the terrain adjacent to the rilles increase from the source area towards the terminal area of the channels, the surfaces will have a negative slope value. Instead, if the depth values decrease towards the terminal area of the channels, the surfaces will have a positive value.
4) *Azimuth:* It approximates the average trend of the rilles, calculated as the horizontal angle between north and the baseline measured clockwise. The straight line of the box, used for the extraction of the sinuosity index has been adopted as baseline.

All the morphological measurements are listed in Table 1 (Appendix 1), where the localization, expressed in latitude and longitude, is provided.

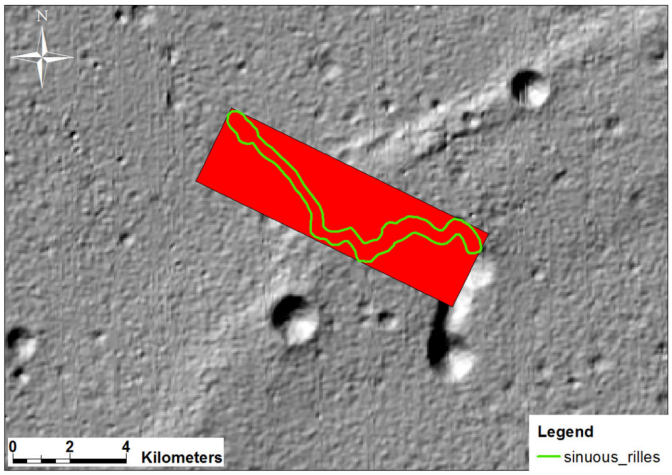

Fig. 7. Image shows the graphic operations performed on sinuous rilles to obtain the straight line value of the channel. The rectangle enclosing the channel has been created as oriented bounding box, and it provides the straight line value of each sinuous rille.

IV. Results and Discussion

A. Global Results

The analysis-based onbWAC and SLDEM2015 images resulted in the detection, mapping and measurement of 51 distinct sinuous rilles (see Fig. 8, and Appendix 2). These features include 37 simple channels (18 new features with respect to [6]), and a sample of 14 new features that represent complex rille systems, as defined in §I. The identified sinuous rilles have different morphological and morphometric characteristics, with varying length, width, depth, slope, and sinuosity values (see Fig. 9).

Sinuous rilles' length range from 3.1 to 207.2 km, with 94% of them having a length shorter than 100 km [see Fig. 9(a)]. These fluctuations in length may be ascribed to the different lava eruption mechanisms. Longer rilles are likely associated with continuous and prolonged flows lasting for a longer time [2], [26].

Sinuous rilles' width are observed to span from 331 m to 2.8 km, with 76% of the rilles characterized by a width less than 1 km [see Fig. 9(b)]. The highest width values are detected in sinuous rilles located in the highlands. Moreover, it can be noticed that these values show significant variations along the length of each channel, specifically for the sinuous rilles with a high mean value of width, as in Fig. 6. Indeed, the averages of the measured widths and the standard deviation of each set of measures show a logarithmic correlation ($R^2 = 0.78$). This behavior demonstrates that for low values of width the sinuous rille is more regular than for high value.

Channel depths are observed to range from 7.9 to 601.5 m, with 62% of them characterized by values less than 100 m [see Fig. 9(c)]. Highest depths are found in sinuous rilles located in the highlands (similarly to what observed for the width). Depth values acquired at several points along the length of each sinuous rille showed significant variations and an average standard deviation of 72.23. This variability has been observed in numerous channels located in the maria and in the transition areas with the highlands. Depth variations in the transition areas between maria and highlands may be related to the different composition of substrate materials, that are less resistant than the ones in the highlands. The variations of depth along each rilles located in the maria, could be related to any subsequent lava flooding on these areas, confirming the data observed in detail on the Rima Marius [26]. Moreover, the variability of the depth values along a rille can be explained with a mechanism of mechanical and thermal erosion [8].

The regional slopes values range from $-5.0°$ to $+3.5°$, with 94% of slopes less than 1.0° (almost flat terrain). The negative or positive sign depends on the trend of the elevations of the surface around the sinuous rilles, starting from the elevation of the source area of the channels. Up to 36% of the observed sinuous rilles reside on positive slopes, suggesting that modification of the surfaces have likely occurred after their formation. The majority of sinuous rilles residing on positive slopes lack a visible source area, and thus the lava flow direction can be determined based on the variations in width and depth values of the channels (see Fig. 10). In this regard, since lava erosion potential tends to decrease with increasing distance from the source area, also width and depth values are expected to decrease in terminal areas of the channels. Sinuous rilles on positive slopes are located in the craters and in maria regions. Positive slopes in the craters are probably the result of surfaces tectonic adjustment after the impact events. Positive slopes in maria are detected for sinuous rilles located at the edge of basins or in association with wrinkle ridges, which cause tectonic deformations of the terrain.

Sinuosity index values are observed to range from 1.03 to 2.43, with 12% of these greater than 1.5 and with 18% less than 1.1.

Further analysis of width and depth average values has been done considering the distribution of sinuous rilles in the three main geomorphologic units: Maria; craters; and highlands [see Fig. 11(a), and (b)]. The number of identified sinuous rilles in the maria regions, in the craters and in the highlands, are, respectively, 25, 13, and 24 rilles.

The plots enhances clear differences of width and depth values of the sinuous rille in the three specific areas. In maria regions, the median values of width and depth are lower than in the other units, and the distributions are more homogeneous rather than in the craters and highlands.

These values can confirm that the composition and the geomorphological structure of the region may affect the evolution of the rille. In maria regions, the flat landscape and the lava flows are extremally more monotonous than in highlands and craters. The variability of these geological characters are particularly clear in the distribution of the parameters in the highlands, where the range of values is very large, and positive outliers can be observed.

Moreover, the channel geometry, calculated as the ratio between the ½ width and depth of the rilles, has been extracted. Values of this shape index range from 1 (semicircular shape of the channel), to 12.2 (a high shallow channel). This morphometric parameter can be used in volcanology studies to model the rheological behavior of the lavas flowing into the channels

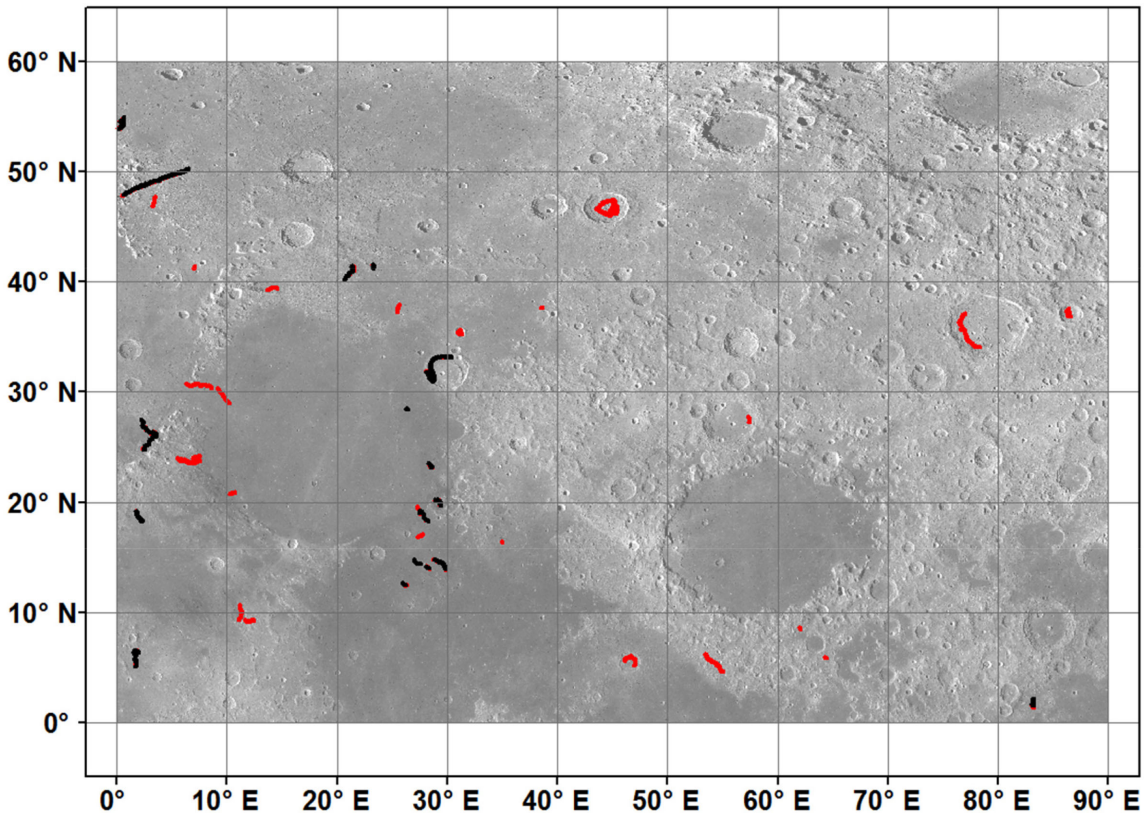

Fig. 8. WAC image shows the distribution of the identified sinuous rilles in the area. The channels in red represent the 32 newly identified features with respect to previous work (in black). (This map is provided also as Appendix, map 1).

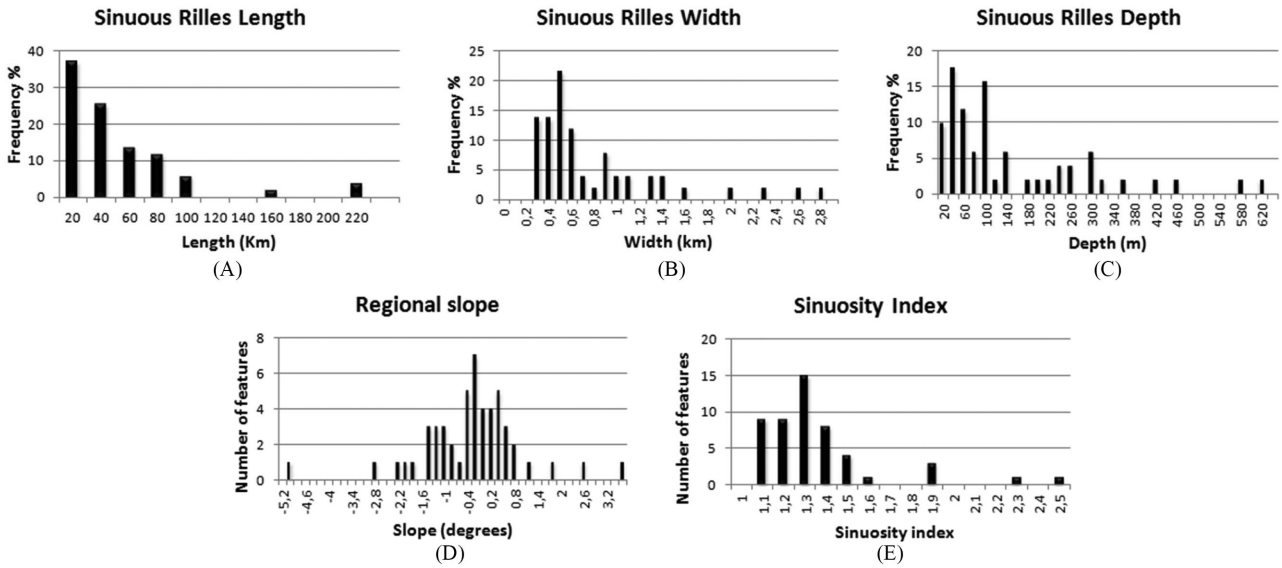

Fig. 9. Frequency graphs of the measured sinuous rilles (a) lengths, (b) widths, (c) depths, (d) slopes, and (e) sinuosity index values. Each bar in length, width and depth graphs represents the frequency (%) of sinuous rilles observed within the corresponding ranges of 20 km, 0.1 km, and 20 m, respectively. Each bar in regional slope and sinuosity index graphs represents the number of features observed within the corresponding ranges of 0.2° and 0.1, respectively.

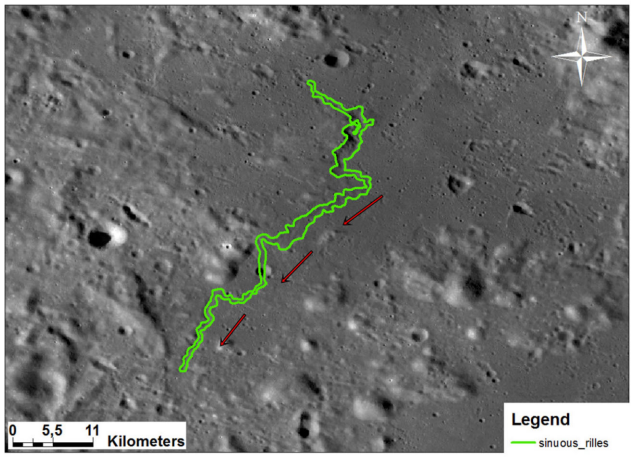

Fig. 10. Example of a sinuous rille on a surface with a positive slope value. In this case, the channel (feature in this WAC image centered at 40.9° N, 21.2° E) lacks a visible source area, and thus the native direction of regional slope is determined based on the variations in width and depth values, that tend to decrease from the north to the south area of the rille as shown by the red arrows.

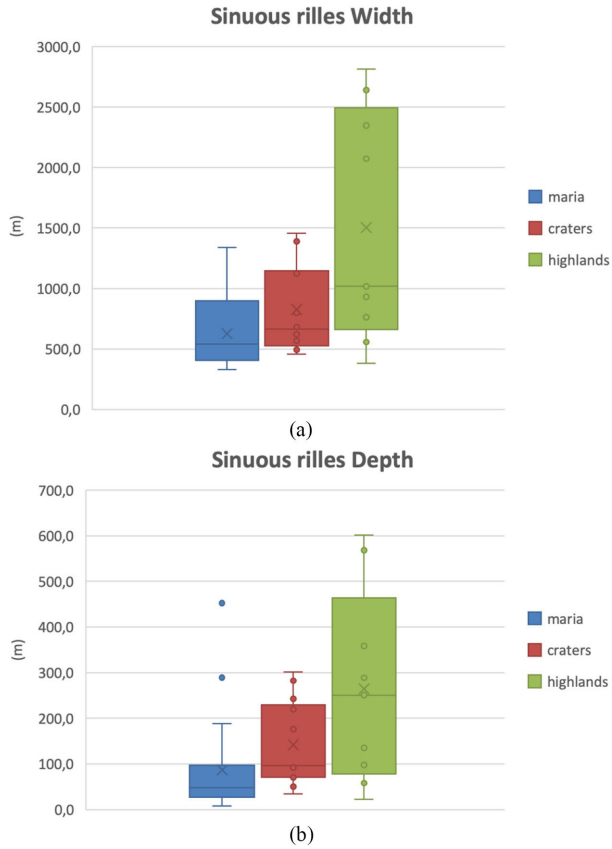

Fig. 11. Distribution of the (a) width and (b) depth average values of the sinuous rilles in the geomorphological units of the study area.

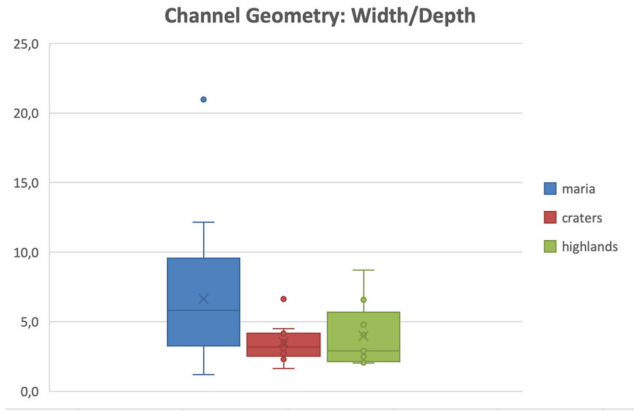

Fig. 12. Distribution of the values of the channel geometry of the sinuous rilles into the three units.

[41]. Moreover, the variability of this geometry can support the interpretation of the lithological characteristics of the eroded rock layer. The distribution of these values is represented in Fig. 12. It can be seen that the highest values of this index are relative to the maria regions, suggesting a wide extension of the rilles and a thin erosion capacity. These values can be interpreted as a resistance to a linear erosion of the consolidated lavas that constitute the maria regions. On the other hand, the low values of this index in the craters and highlands can demonstrate a higher rate of erodibility on that regions. These observation can be confirmed by the distribution of the sinuosity index of the rilles in the three regions (see Fig. 13). Highest values can be seen in the craters, where the discontinuities of the lavas surfaces are common, due to the melting and cooling stages.

Eventually, the analysis of the azimuth distribution has been carried out with the objective of verifying if preferred trends were recognizable. Furthermore, these trends were compared with the orientations of existing linear geological features (graben traces, lineaments, and ridge crests), referred to the global geologic map of the Moon [27].

All the values were divided into three families, according to their presence in the three geological units, i.e., maria, craters, and highlands, and were plotted in Rose diagrams [see Fig. 14(a)–(e), and (f)]. As it can be noted, the distribution of the values range in almost all directions (from 0° to 180°), and it is difficult to identify preferred orientation trends. In the maria regions and in the craters [see Fig. 14(a) and (c))] a favorite north-south direction can be considered as specific of these regions. Indeed, in the highlands, it is not observed. Again, some favorite directions in the highlands [see Fig. 14(e)] can be observed also in the maria.

Moreover, the comparison with the orientations of existing geological linear features highlights that the behavior of the sinuous rilles can be considered almost independent from the other geological structures [see Fig. 14(b), (d), and (f)]. This consideration could suggest the importance to date the sinuous rilles and relate them to the geological history of the lunar volcanism.

B. Observed Trends

Observations have been made by analyzing the existing relationships between the different morphometric parameters, in order to identify any morphological trends. Width and depth

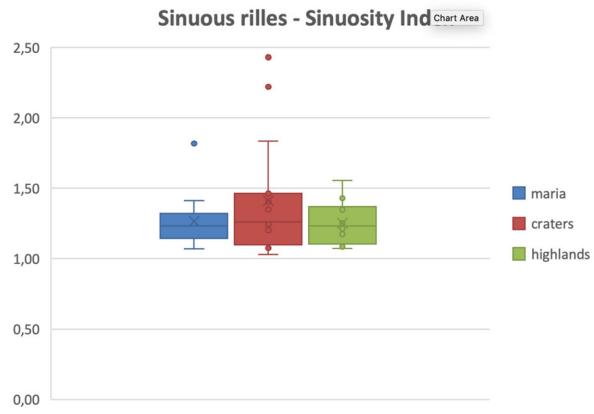

Fig. 13. Distribution of the (a) width and (b) depth average values of the sinuous rilles in the geomorphological units of the study area.

values show a linear correlation (see Fig. 15). This trend is consistent with the hypothesis that lava erosion acts proportionally in both vertical and horizontal directions during the eruptions required for sinuous rilles formation.

Moreover, the graph in Fig. 15 highlights that this correlation decreases for the longest rilles. These forms are mainly developed into the maria, where the calculated channel geometry provides a wide and thin rille (see Fig. 12).

The relationships between the different parameters have been analyzed separately for *simple channels* and for *complex rille systems*. The correlation graphs of width-depth and sinuosity-slope show the same relationships between the parameters resulting from the analysis of all features (see Fig. 16).

Furthermore, width and depth values, related to those sinuous rilles located in the craters, in the highlands, and in the maria regions have been analyzed. The results are similar to the same obtained for all features. Only the width-depth correlation graph of the channels located in maria regions shows a less linear relationship between the two parameters (see Fig. 17). This fact is consistent with the measured standard deviation values of the two parameters. Indeed, these showed large variations in depths values compared to the ones observed in width values. These variations could be due the origin of the channel, due to a thermal and mechanical erosion, as suggested in studies on similar processes on Venus [8].

The relationship between the sinuosity index and the slope values of the surfaces on which sinuous rilles formed has been analyzed. These two parameters have a complex relationship in terrestrial fluvial channels, which are expected to become sinuous at slopes of 0.11° and continue developing meanders until a sinuosity index maximum value of 1.25 [42]. According to this model, beyond the slope of 0.92 the channels would become braided. This relationship also depends on other parameters, such as the sediment load [6]. As the gravity and compositions of the flowing lava on the Moon are different from the ones on Earth, the relationship between the sinuosity index and slope could change substantially. Indeed, the correlation between the

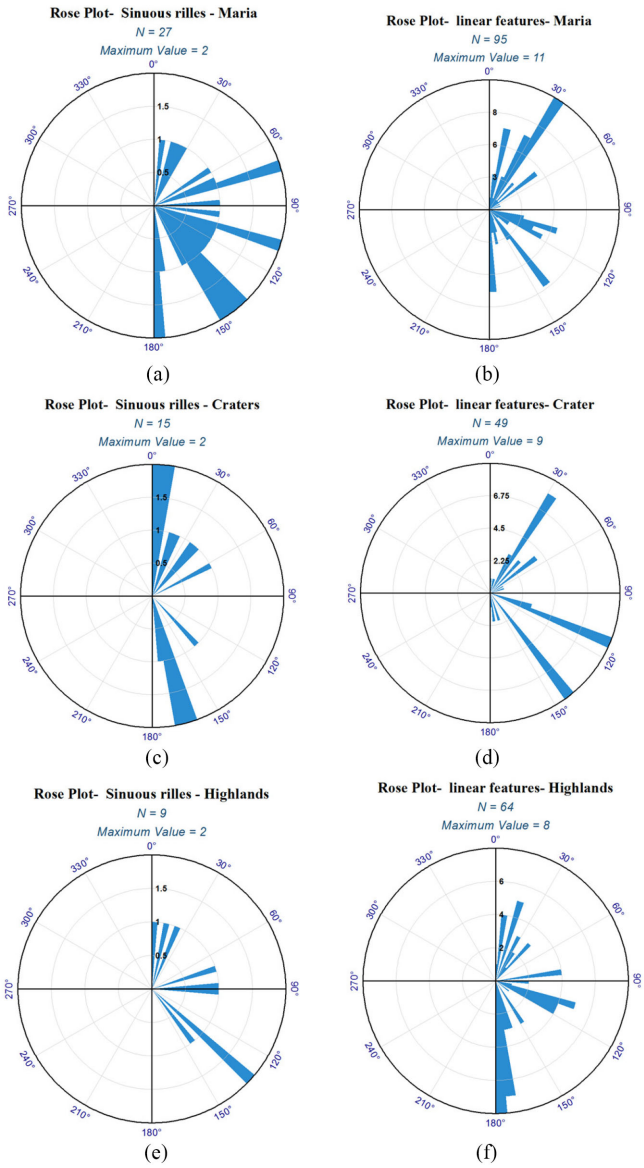

Fig. 14. Rose diagrams of the distribution of the azimuth of the sinuous rilles and linear geological features into the three geological units: (a) and (b) maria; (c) and (d) craters; and (e) and (f) highlands.

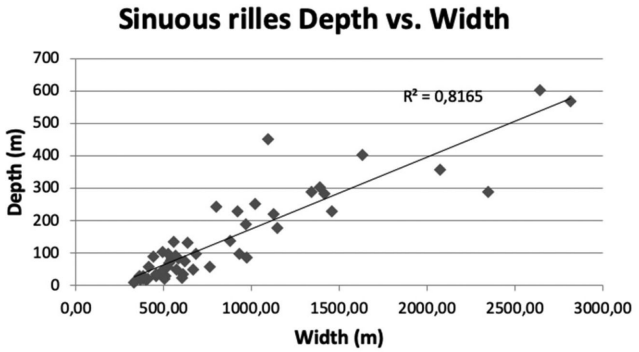

Fig. 15. Graph shows the linear relationship between depth and width values of the identified sinuous rilles. The graph shows a linear relationship ($R^2 = 0.82$) between the two parameters, which confirms the idea that lava erosion efficiency acts proportionally in both vertical and horizontal directions.

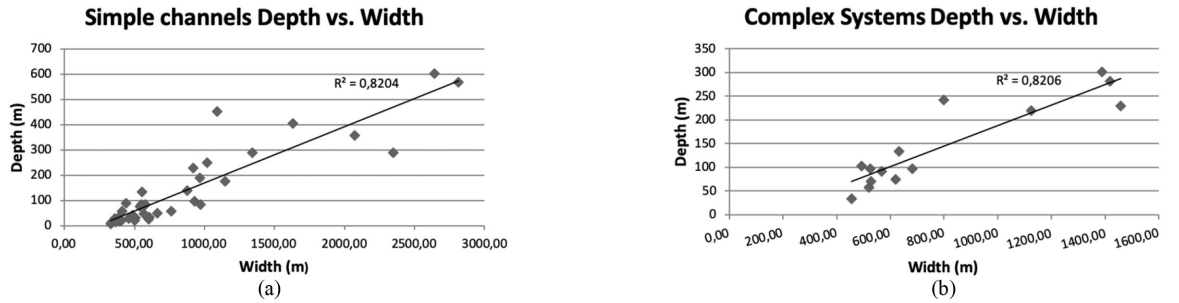

Fig. 16. Simple channels and complex rille systems correlation graphs. These graphs show the relationship between the morphometric parameters separately (a) for simple channels and (b) for complex rille systems. The observed relationships are the same of that resulting by the analysis of all sinuous rilles. Depth and width values have a linear relationship.

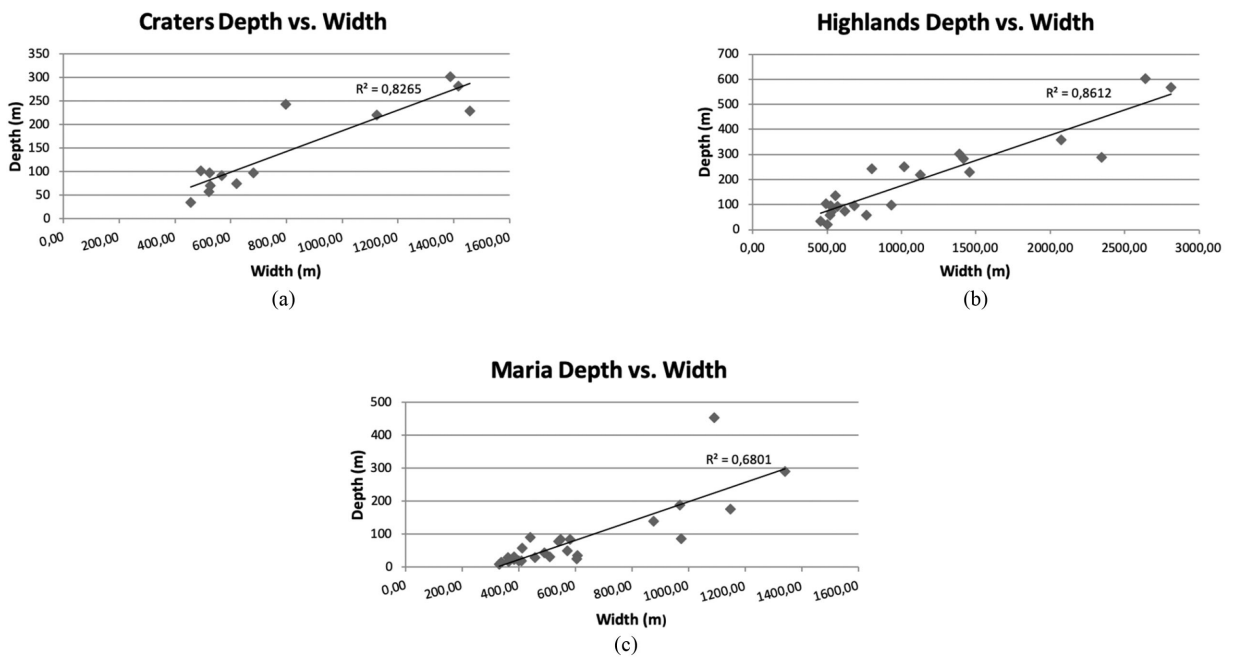

Fig. 17. Correlation graphs Depth - Width based on the location of the identified sinuous rilles, that are observed in the (a) craters, (b) in highlands, and (c) in maria regions. The graphs show that the relationship between depth and width values is less linear in maria regions in reference to the other location zones.

sinuosity and the (positive) slope shows that there is no correlation, according to the observation of previous authors [6].

V. Conclusion

The analysis conducted in this article has shown that sinuous rilles are rather complex features, with different morphological and morphometric characteristics.

In this article, a total of 51 sinuous rilles have been recognized in the study area, 18 of which are new, improving the previous catalogue [6]. The observed morphologic variability, highlighted by the measured parameters, depends both on the eruptive mechanism, and on the surface compositional characteristics in which sinuous rilles formed.

The first step of the study was focused on the identification of these morphologies. The visual recognition was adopted as main methodology of interpretation, due to technological limit of the available data, mainly in terms of spatial resolution. The automatic extraction of morphometric parameters from DEM allowed to obtain the following values for each sinuous rille: width, depth, length, sinuosity index, and regional slope. Moreover, the channel geometry and the azimuth of each rille has been used to obtain more information on its origin and evolution.

All the morphometric values, expressed as the average value of each variable, have been plotted and compare each other', to understand the distribution of their values and the general characteristics of the studied morphologies. From these first observations, differences between their parameters have been highlighted, and the need to divide them according to the geological unit where they formed emerged. For this purpose, morphometric parameters have been analyzed dividing them into three families, referred to maria, craters, and highlands regions.

The importance of the substrate composition in the evolution of these features emerged from the variations in width and

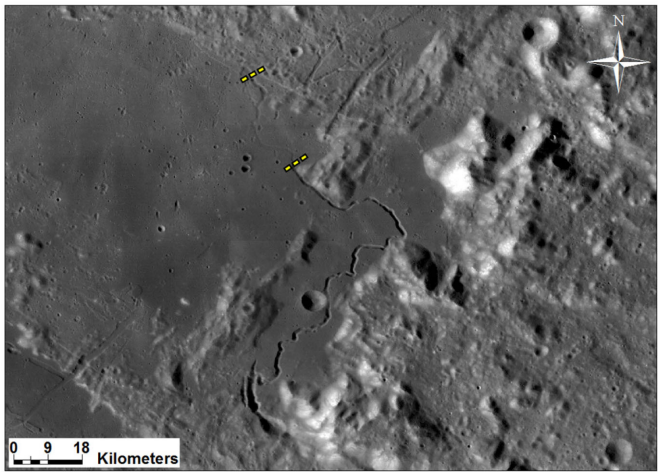

Fig. 18. Example of a sinuous rille characterized by partial filling phenomena by subsequent lava flows. The observed rille (feature in WAC image centered at 25.9° N, 2.8° E) have a great difference in width values between the source area and the terminal area showed by the yellow lines.

depth values. The emerged linear relationship between both parameters is consistent with the idea that erosion efficiency acts proportionally in both vertical and horizontal directions.

This relationship, clear for low values of depth and width, changes for higher values and, in particular, in maria regions. Indeed, the lower depth values in maria and the resulting wide geometry of the channel are due to the presence of more resistant rocks, such as basalts. By these observations, the trend of erosion results strictly connected with the lithology of the eroded layer, providing useful geological information. The linear correlation in highlands for most of the rilles is related to more erodible rock and abundant loose layer of regolith, which is therefore eroded more easily than basaltic lavas. Into the craters, this linear correlation can be explained with the presence of lineaments and discontinuities on the surface, which allows thermal and mechanical erosion of the channel.

Moreover, the observed less linear relationship in the high values od width into maria could be connected to three different factors.

1) The rheological behavior of the flowing lavas during the thermal erosion of the basaltic rock, as discussed earlier.
2) A constructive genesis of sinuous rilles.
3) Partial filling phenomena of the channels by subsequent lava flows.

The hypothesis of a constructive genesis requires further investigation with higher resolution data, to identify the levees created by sinuous rilles' formation process. Partial filling phenomena by subsequent lava flows probably occurred in some sinuous rilles located in maria (see Fig. 18). This is also confirmed by large variations in the depth values between the source area and the terminal area of the channels. Instead, these variations were not measured in width values, and this fact confirms the hypothesis.

The control of the composition of the substratum on the evolution of the sinuous rilles, has been confirmed by the sinuosity values. The highest and most variable sinuosity values have been found into the craters. Although the median value is almost the same, in maria regions the sinuosity is more uniform than into the craters and highlands. The relationship between sinuosity index and slope values did not show any significative trend.

Instead, positive values of the regional slope around 36% of the rilles, suggest a tectonic activity of deformation of the surfaces after the creation of these rilles.

Azimuth values, analyzed separately in the three geological units and compared with the linear geological features do not seem to give indication of preferred directions. These results could suggest further analysis for proposing different ages to the creation and evolution of the sinuous rilles.

The analyses carried out separately for simple channels and for complex rille systems did not show large differences between the behaviors of these two features. The measured morphometric parameters of complex rille systems showed a similar trend of simple channels. This result may challenge the idea that the main control factor of complex rille systems formation is tectonic. These morphologies are probably the result of tectonic deformations associated with lava thermal erosion. Indeed, tectonic control is visible by visual interpretation, because the course of these systems appears angular and less sinuous than simple channels, while the lava thermal erosion control results by measured parameters' values.

The results of this article highlight that these morphologies have rather complex and still unclear formation and evolution processes. The complexity of sinuous rille morphology doesn't allow us to perform an automatic detection alone, because their identification still requires an accurate visual interpretation, and the spatial resolution of the DEM, in the study area, is the main limit.

The information extracted from visual interpretation and automatic detection have been integrated to provide suggestions on the origin and evolution of sinuous rilles. In this article, a particular attention has been done to the relationship between the morphometric parameters values and the geological units. This approach allowed to provide new suggestions for future improvement on the knowledge of these "*enigmatic lineaments.*"

ACKNOWLEDGMENT

This work was realized in the framework of "Moon mapping project," (2015–2019). The main acknowledgments go to the Italian Space Agency and the Center of Space Exploration of China Ministry of Education which have promoted, funded and supported this project. The authors would also thank all those colleagues and students who have been supporting in some way the research or the activities.

REFERENCES

[1] G. Hulme, "Turbulent lava flow and the formation of lunar sinuous rilles," *Modern Geol.*, vol. 4, pp. 107–117, 1973.
[2] D. M. Hurwitz, J. W. Head, L. Wilson, and H. Hiesinger, "Origin of lunar sinuous rilles: Modeling effects of gravity, surface slope, and lava composition on erosion rates during the formation of Rima Prinz," *J. Geophys. Res. Planets*, vol. 117, no. E12, Dec. 2012, doi: 10.1029/2011JE004000.
[3] V. R. Oberbeck, "On the origin of Lunar sinuous rilles," *Modern Geol.*, vol. 1, pp. 75–80, 1969, [Online]. Available: https://ci.nii.ac.jp/naid/10010295095/en/

[4] R. Greeley, "Lunar hadley rille: Considerations of its origin," *Science*, vol. 172, no. 3984, pp. 722–725, 1971, doi: 10.1126/science.172.3984.722.
[5] V. Gornitz, "The origin of sinuous rilles," *Moon*, vol. 6, pp. 337–356, 1973, doi: 10.1007/BF00562210.
[6] D. M. Hurwitz, J. W. Head, and H. Hiesinger, "Lunar sinuous rilles: Distribution, characteristics, and implications for their origin," *Planet. Space Sci.*, vol. 79–80, pp. 1–38, May 2013, doi: 10.1016/j.pss.2012.10.019.
[7] G. Hulme, "A review of lava flow processes related to the formation of lunar sinuous rilles," *Geophys. Surv.*, vol. 5, no. 3, pp. 245–279, Oct. 1982, doi: 10.1007/BF01454018.
[8] S. Oshigami, N. Namiki, and G. Komatsu, "Depth profiles of venusian sinuous rilles and valley networks," *Icarus*, vol. 199, no. 2, pp. 250–263, 2009, doi: https://doi.org/10.1016/j.icarus.2008.10.012.
[9] G. Komatsu, "Rivers in the solar system: Water is not the only fluid flow on planetary bodies," *Geography Compass*, vol. 1, no. 3, pp. 480–502, 2007, doi: 10.1111/j.1749-8198.2007.00029.x.
[10] G. Komatsu and H. Hargitai, "Sinuous Rille," in *Encyclopedia of Planetary Landforms*, New York, NY, USA: Springer, 2014, pp. 1–9.
[11] D. A. Williams, A. H. Wilson, and R. Greeley, "A komatiite analog to potential ultramafic materials on Io," *J. Geophys. Res. Planets*, vol. 105, no. E1, pp. 1671–1684, 2000, doi: 10.1029/1999JE001157.
[12] M. Scaioni *et al.*, "The 'Moon Mapping' project to promote cooperation between students of Italy and China," *Int. Arch. Photogramm. Remote Sens. Spat. Inf. Sci. - ISPRS Arch.*, vol. 41, pp. 71–78, 2016, doi: 10.5194/isprsarchives-XLI-B6-71-2016.
[13] M. Scaioni *et al.*, "Recognition of landslides in lunar impact craters," *Eur. J. Remote Sens.*, vol. 51, no. 1, pp. 47–61, Jan. 2018.
[14] D. M. Blair *et al.*, "The structural stability of lunar lava tubes," *Icarus*, vol. 282, pp. 47–55, 2017, doi: https://doi.org/10.1016/j.icarus.2016.10.008.
[15] J. Haruyama *et al.*, "Possible lunar lava tube skylight observed by SELENE cameras," *Geophys. Res. Lett.*, vol. 36, no. 21, 2009, doi: 10.1029/2009GL040635.
[16] J. N. Rasera, J. J. Cilliers, J. A. Lamamy, and K. Hadler, "The beneficiation of lunar regolith for space resource utilisation: A review," *Planetary Space Sci.*, vol. 186, 2020, Art. no. 104879, doi: https://doi.org/10.1016/j.pss.2020.104879.
[17] P. D. Spudis, G. A. Swann, and R. Greeley, "The formation of Hadley Rille and implications for the geology of the Apollo 15 region.," *Lunar Planet. Sci. Conf. Proc.*, vol. 18, pp. 243–254, Jan. 1988, [Online]. Available: https://ui.adsabs.harvard.edu/abs/1988LPSC…18..243S.
[18] T. Murase and A. R. McBirney, "Viscosity of Lunar Lavas," *Science*, vol. 167, no. 3924, pp. 1491–1493, 1970, doi: 10.1126/science.167.3924.1491.
[19] J. Siewert and C. Ferlito, "Mechanical erosion by flowing lava," *Contemporary Phys.*, vol. 49, no. 1, pp. 43–54, Jan. 2008, doi: 10.1080/00107510802077388.
[20] D. A. Williams, R. C. Kerr, C. M. Lesher, and S. J. Barnes, "Analytical/numerical modeling of komatiite lava emplacement and thermal erosion at perseverance, Western Australia," *J. Volcanol. Geothermal Res.*, vol. 110, no. 1, pp. 27–55, 2001, doi: https://doi.org/10.1016/S0377-0273(01)00206-2.
[21] M. H. Carr, "The role of lava erosion in the formation of lunar rilles and Martian channels," *Icarus*, vol. 22, no. 1, pp. 1–23, May 1974, doi: 10.1016/0019-1035(74)90162-6.
[22] L. Wilson and J. W. Head, III, "Ascent and eruption of basaltic magma on the Earth and Moon," *J. Geophys. Res. Solid Earth*, vol. 86, pp. 2971–3001, Apr. 1981.
[23] D. A. Williams, S. A. Fagents, and R. Greeley, "A reassessment of the emplacement and erosional potential of turbulent, low-viscosity lavas on the Moon," *J. Geophys. Res. Planets*, vol. 105, pp. 20189–20205, 2000, doi: 10.1029/1999JE001220.
[24] V. R. Oberbeck, R. Greeley, R. B. Morgan, and M. J. Lovas, "Lunar rilles: A catalog and method of classification," NASA TM-X-62088, p. 83, 1971.
[25] P. H. Schultz, "Floor-fractured lunar craters," *Moon*, vol. 15, no. 3, pp. 241–273, Sep. 1976, doi: 10.1007/BF00562240.
[26] C. E. Roberts and T. K. P. Gregg, "Rima Marius, the moon: formation of lunar sinuous rilles by constructional and erosional processes," *Icarus*, vol. 317, pp. 682–688, Jan. 2019, doi: 10.1016/j.icarus.2018.02.033.
[27] C. M. Fortezzo, P. D. Spudis, and S. L. Harrel, "Release of the digital unified global geologic map of the moon at 1:5,000,000- scale," in *Proc. 51st Lunar Planetary Sci. Conf., Lunar Planetary Inst.,* 2020, [Online]. Available: https://www.hou.usra.edu/meetings/lpsc2020/pdf/2760.pdf
[28] D. E. Wilhelms, *The Geologic History of the Moon*. New York, NY, USA: Springer, 1987.
[29] R. Jaumann *et al.*, "Geology, geochemistry, and geophysics of the Moon: Status of current understanding," *Planetary Space Sci.*, vol. 74, no. 1, pp. 15–41, 2012, doi: https://doi.org/10.1016/j.pss.2012.08.019.
[30] S. Vijayan, S. Mohan, and S. S. Murty, "Lunar regolith thickness estimation using dual frequency microwave brightness temperature and influence of vertical variation of $FeO+TiO_2$," *Planetary Space Sci.*, vol. 105, pp. 123–132, 2015, doi: https://doi.org/10.1016/j.pss.2014.11.017.
[31] M. S. Robinson *et al.*, "Lunar reconnaissance orbiter camera (LROC) instrument overview," *Space Sci. Rev.*, vol. 150, no. 1, pp. 81–124, Jan. 2010.
[32] M. K. Barker, E. Mazarico, G. A. Neumann, M. T. Zuber, J. Haruyama, and D. E. Smith, "A new lunar digital elevation model from the lunar orbiter laser altimeter and SELENE terrain camera," *Icarus*, vol. 273, pp. 346–355, Jul. 2016.
[33] I. V. Florinsky, "An illustrated introduction to general geomorphometry," *Prog. Phys. Geograph Earth Environ.*, vol. 41, no. 6, pp. 723–752, 2017, doi: 10.1177/0309133317733667.
[34] R. Dikau, "Case studies in the development of derived geomorphic maps," *Geol. Jahrbuch*, vol. A104, pp. 329–338, 1988.
[35] Z. Luo and Z. Kang, "Automatic extraction of lunar impact craters from Chang'E images based on Hough transform and RANSAC," in *Proc. 2nd ISPRS Int. Conf. Comput. Vis. Remote Sens.*, 2016, vol. 9901, pp. 111–116, doi: 10.1117/12.2234683.
[36] Z. Kang, Z. Luo, T. Hu, and P. Gamba, "Automatic extraction and identification of lunar impact Craters based on optical data and DEMs acquired by the Chang'E satellites," *IEEE J. Sel. Top. Appl. Earth Observ. Remote Sens.*, vol. 8, no. 10, pp. 4751–4761, Oct. 2015.
[37] M. T. Melis, F. Mundula, F. Dessì, R. Cioni, and A. Funedda, "Tracing the boundaries of Cenozoic volcanic edifices from Sardinia (Italy): A geomorphometric contribution," *Earth Surf. Dyn.*, vol. 2, no. 2, 2014, doi: 10.5194/esurf-2-481-2014.
[38] A. Vacca *et al.*, "A GIS based method for soil mapping in Sardinia, Italy: A geomatic approach," *J. Environ. Manage.*, vol. 138, pp. 87–96, 2014, doi: 10.1016/j.jenvman.2013.11.018.
[39] S. Vijayan, K. Vani, and S. Sanjeevi, "Topographical analysis of lunar impact craters using SELENE images," *Adv. Space Res.*, vol. 52, no. 7, pp. 1221–1236, 2013, doi: https://doi.org/10.1016/j.asr.2013.06.025.
[40] R. Dikau, "The application of a digital relief model to landform analysis in geomorphology," in *Three Dimensional Applications in Geographical Information Systems*, J. F. Raper, Ed., London, U.K.: Taylor & Francis, 1989, pp. 51–77.
[41] E. Lev and M. R. James, "The influence of cross-sectional channel geometry on rheology and flux estimates for active lava flows," *Bull. Volcanol.*, vol. 76, no. 7, Jun. 2014, doi: 10.1007/s00445-014-0829-3.
[42] S. A. Schumm and H. R. Khan, "Experimental study of channel patterns," *Nature*, vol. 233, no. 5319, pp. 407–409, Oct. 1971.

Sabrina Podda received the B.S. degree in geological sciences and the M.S. degree in geological sciences and technologies from the University of Cagliari, Cagliari, Italy, in 2015 and 2018, respectively.

She with the Department of Chemical and Geological Science, University of Cagliari, on the geomorphological study of the lunar surface through remote sensing data.

Maria Teresa Melis received the graduate degree in geology, in 1985, and the Ph.D. degree in remote sensing application to arid and semiarid geomorphological mapping, in 1995.

She is an Adjunct Professor with GIS, and the Technical Responsible for the "TeleGIS" Remote Sensing Laboratory, University of Cagliari, Cagliari, Italy. She is Co-Chair of the III Commission Remote sensing with ISPRS (International Society for Photogrammetry and Remote Sensing), WGIII 1—Thematic Information Extraction. She has authored or coauthored more than 50 papers and contribution in books. Her research interests include remote sensing applied to geological/land cover/geomorphological analysis in remote areas (cold and hot arid lands).

Dr. Melis is Member of the Scientific Council of ASITA (Federation of Italian Scientific Associations in Environmental and Land Information). She was the Vice President of the Italian Association of Remote Sensing. Authored or coauthored more than 50 papers and contribution in books.

Claudia Collu received the B.S. degree in geological sciences and the M.S. degree in geological sciences and technologies from the University of Cagliari, Cagliari, Italy, in 2015 and 2018, respectively. In 2019, she received the 2nd level Specializing master's degree in geomatics from University of Siena, Siena, Italy.

Valentino Demurtas is working toward the Ph.D. degree in earth science, topic research title: Deep-seated gravitational slope deformations of central Sardinia, evolutionary dynamics and innovative monitoring techniques.

He was a Visiting Ph.D. student in earth science with Norway geological survey (NGU), Trondheim, Norway. His research interests include deep landslides, coastal landslides, morphotectonic, UAV Photogrammetry, InSAR, geomorphological mapping, 3-D geological modeling, and landslide monitoring.

Francesco Onorato Perseu received the B.S. degree in geological sciences and the M.S. degree in geological sciences and technologies from the University of Cagliari, Cagliari, Italy, in 2015 and 2018, respectively.

He has received a research fellowship with the University of Cagliari, Italy, in 2018 on the calibration of SAR datasets with ground data.

Maria Teresa Brunetti received the Master degree in physics, in 1991, with a thesis on "Cosmic antihelium detection in a silicon calorimete" and the Ph.D. degree in earth sciences and geotechnologies, in 2014 with a thesis on "Statistics of terrestrial and extraterrestrial landslides".

She is a Research Scientist with the Italian National Research Council, the Research Institute for Geo-Hydrological Protection, Perugia, Italy. She worked in the fields of astrophysics and particle physics in international collaborations with National Aeronautics and Space Administration, European Space Agency, and Conseil Européen pour la Recherche Nucléaire. She currently works on natural hazards, and on the terrestrial and planetary geomorphology. She is co-author of 60 papers in ISI journals, and seven contributions in books.

Marco Scaioni received the graduate degree in civil engineering, in 1995, and Ph.D. degree in geodetic and mapping sciences from Politecnico di Milano, Milan, Italy, in 1999.

He is currently an Associate Professor of Geomatics at Politecnico di Milano with the Department of Architecture, Built Environment and Construction Engineering, Milano, Italy, where is the Head of ABC-PhD programme. From 2011 to 2014, he was a Professor with Tongji University, College of Surveying and Geo-Informatics, Shanghai, China. His research interests include mainly close-range photogrammetry, terrestrial laser scanning, satellite and terrestrial remote sensing, geo-hazards, and geoscience research.

Dr. Scaioni is the Chairman of the ISPRS Working Group III/5 on "Information Extraction from LiDAR Intensity Data during 2016–2021. He is an Associate Editor for the *ISPRS Journal of Photogrammetry and Remote Sensing* (Elsevier) and *Applied Geomatics* (Springer).